Research on icing behavior and ice adhesion testing of icephobic surfaces

Heli Koivuluoto[1], Christian Stenroos[1], Riku Ruohomaa[1], Giovanni Bolelli[2], Luca Lusvarghi[2], Petri Vuoristo[1]
[1]Tampere University of Technology (TUT), Department of Materials Science, Tampere, Finland, [2]University of Modena and Reggio Emilia (UNIMORE), Department of Engineering "Enzo Ferrari", Modena ,Italy
heli.koivuluoto@tut.fi

***Abstract*: Surface engineering shows potential to provide sustainable approach to icing problems. Currently several passive anti-ice mechanisms adoptable to coatings are known but further research is required to proceed for practical applications. Icing wind tunnel and centrifugal ice adhesion test equipment enable the evaluation and development of anti-ice and icephobic coatings for e.g., wind turbine applications but also other growing players in arctic environment e.g. oil, extractive and logistic industries. This research is focused on the evaluation of icing properties of various surfaces.**

Keywords: ice adhesion, icing wind tunnel, ice accretion, coatings, surface properties

LEGEND AND ABBREVIATIONS

CA	*Contact angle*
F	*Fluorine*
FEP	*Fluorinated ethylene propylene*
IA	*Ice adhesion*
LWC	*Liquid Water Content*
PTFE	*Polytetrafluoroethylene*
PU	*Polyurethane*
VMD	*Volume median diameter*

INTRODUCTION

On-going climate change, opening of new logistic routes, energy and mineral resources as well as increasing tourism feed the growing activity in cold climate regions. One of the major challenges for operations in these areas is ice and snow accretion. Icing reduces safety, operational tempo, productivity and reliability of logistics, industry and infrastructure. Figure 1 shows examples of an ice accretion on the problematic parts such as on wind turbine blade leading edge and on vessel.

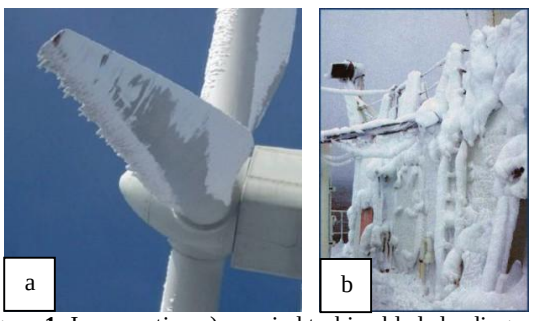

Figure 1: Ice accretion a) on wind turbine blade leading edge [1] and b) on vessel [2].

Surface engineering shows potential to sustainable approach to icing problems. Passive anti-ice coatings can hinder ice formation and icephobic surfaces reduce the adhesion of accreted ice. Current commercial coatings with icephobic characteristics rely on hydrophobicity, releasing of lubricant or melting point depressants and ablation. Currently, research is additionally carried out on icephobic potential of superhydrophobic surfaces [3], phase change materials [4], slippery liquid infused surfaces [5], anti-freeze proteins [6] and surface morphology [3,7]. All these anti-ice mechanisms show promising results in reducing ice accretion and adhesion. Nevertheless, so far these are functional only in specific icing conditions for a limited amount of time. However, the wear resistance of these coatings is poor and thus, the current coatings are practical only in limited applications or the icephobic effect is insufficiently significant [8]. Ideal icephobic surface should have also anti-ice characteristics. It should work in three different stages of ice formation. Ideal icephobic surface should 1) minimize accumulation of water on the surface by reducing interactions of the surface and incoming water, 2) inhibit heterogeneous ice nucleation and 3) weaken the adhesion of ice on the surface [9].

As an example, there are three main icing mechanisms for wind turbine applications: 1) in-cloud icing, 2) precipitation icing (wet snow, freezing rain) and 3) frost formation [10]. The first two mechanisms include supercooled liquid water and the third one condensing water vapor. In-cloud icing is the most detrimental icing mechanism for wind turbines [11]. It occurs when supercooled water droplets, contained in cloud or fog, hit a surface below 0 ºC and freeze upon impact. In-cloud icing can be divided in two sub-mechanisms based on the macrostructure of resulting ice: rime (soft and hard) icing and glaze icing. In rime icing, water droplets freeze immediately upon impact contact with the surface and form porous ice with white appearance [12]. Soft rime has a feathery appearance, it is formed at cold temperatures, from small droplets, low liquid water content (LWC) and its adhesion is low. Hard rime has more icy appearance but it has still high porosity. Hard rime has higher adhesion and it is formed after slower freezing which, in turn, is due to larger droplets, higher liquid water content, or higher temperature. On the other hand, in glaze icing, part of the water droplets freeze upon impact and the remainder run along the surface before freezing and form smooth and non-porous clear ice.

In order to develop anti-ice or icephobic coatings, test equipment was designed and constructed. Several icing tests have been introduced in literature [13-15]. However, often these tests either include heavy wind tunnels used by aerospace and automotive industry or the tests are extremely simplified and far from practical conditions. Even more, icing tests are not standardized. To make affordable and compact but truthful test facilities for evaluation of icing, it was decided that a small scale icing wind tunnel and an ice adhesion test apparatus be constructed. Both of these items are placed in a climatic room to guarantee constant atmospheric conditions throughout testing.

An icing wind tunnel has a capability to simulate the ice accretion by both in-cloud mechanism (glaze and rime icing) and precipitation icing. With centrifugal ice adhesion test, it is possible to test either bulk-formed ice or atmospherically accreted ice. These test devices enable evaluation and development of anti-ice and icephobic coatings not only for wind turbine applications but also other application fields in arctic environment.

This research focuses on the evaluation of icing properties of various coatings and surfaces. Furthermore, the stress distribution in the ice block during the centrifugal ice adhesion test was modelled by finite elements method in order to understand the interfacial behavior of ice and surface. In addition to ice adhesion, wettability and surface roughness were characterized.

I. Experimental procedure

A. *Icing tests*

For ice testing, an icing wind tunnel was designed and constructed. After ice accretion, the ice adhesion was measured with centrifugal ice adhesion test. Icing behavior is compared with wettability and roughness of the surfaces. Icing tests therefore include ice accretion through a wind tunnel in a cold climate room and ice adhesion measurements by using a centrifugal ice adhesion test, Fig. 2. The ice adhesion test equipment is based on the description by Laforte and Beisswenger [16].

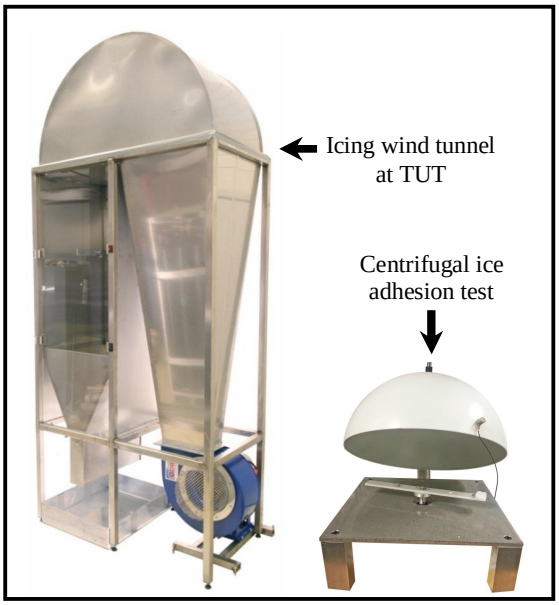

Figure 2: Icing wind tunnel and centrifugal ice adhesion test at TUT.

In the centrifugal ice adhesion test, a plate (340 x 30 mm) with iced area (30 x 30 mm) is rotated with a constant acceleration rate until the ice detaches. Detachment is observed by acceleration sensor. The iced test plate is weighted before and after the test in order to measure the mass of detached ice. When adhesion area is measured and the speed of rotation at the moment of detachment is known, the maximum adhesive shear strength can be calculated. The centrifugal force F can be written as:

$$F = mr\omega^2 = wLhpr\omega^2 \quad (1)$$

Where m is the mass, w is the width, L is length, h is the height and ρ is the density of ice, r is the radius of rotation and ω is angular velocity. It can be seen that centrifugal force is directly proportional to all specimen dimensions. However, width and length do not effect on shear stress τ:

$$\tau = \frac{F}{A} = \frac{wLhpr\omega^2}{wL} = hpr\omega^2 \quad (2)$$

Specification of the icing wind tunnel at TUT is presented in Table 1. Several parameters e.g. nozzle parameters, water droplet size and liquid water content can be varied. By this way, the ice formation can be modified (e.g., rime and glaze ice). The critical factor affecting on the quality and type of ice are the spraying parameters.

Table 1: Specification of the icing wind tunnel at TUT.

Parameters		Min	Max	
Nozzle parameters	P (Liquid)	0	5	bar
	Q (liquid)	0	0.3	l/min
	P (Gas)	0	5	bar
	Q (Gas)	0	150	l/min
Volume median diameter (VMD)	D(V0.5)	25	1000	µm
Flow velocity	v	0	25	m/s
Temperature	T	0	-40	˚C
Nozzle-specimen distance	H	0	1.9	m
Liquid water content	LWC	0	4.2	g/m^3

In this study, icing conditions were selected as rime, normal and glaze ice can be formed. Normal test ice refers to ice which is as close to glaze ice as possible without containing icicles or runback ice. This kind of ice is easy to test due to regular shape of the ice block. It contains approximately 3 vol-% of porosity resulting in translucent appearance.

Rime ice is formed, when clouds or fog containing supercooled droplets freeze immediately upon contact to a surface preserving their spherical form. The glaze ice is formed from larger droplets caused by wet in-cloud icing, freezing rain or drizzle. The droplets that create glaze ice will stay in the liquid state momentary in the contact of the surface, before freezing.

In the present ice accretions, the temperature was chosen as –10 ºC and the flow velocity was set to the maximum 25 m/s. In addition, the nozzle-specimen distance was set to 1.5 m. The different ice types were created by altering the gas pressure. By increasing the pressure to 5.5 bar, the 25 µm VMD for droplets could be achieved (according to nozzle manufacturer: Spraying system Co.) and rime ice created. The glaze ice was accreted with the 2.3 bar corresponding to 40 µm VMD of the droplets. The normal ice was accreted with the 3.5 bar pressure corresponding to 31 µm VMD of the droplets.

B. *Finite element modeling of the centrifugal ice adhesion test*

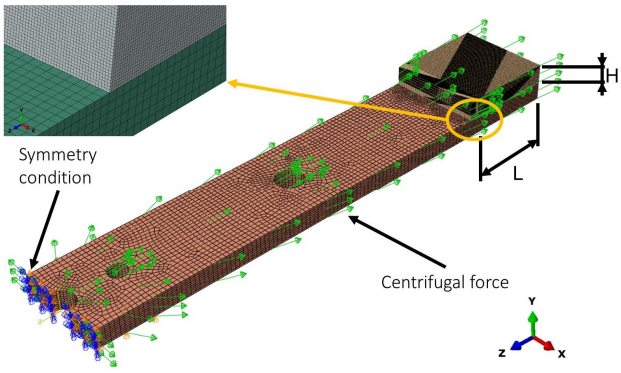

Figure 3: Finite element model of the centrifugal ice adhesion test.

Stress-strain distributions in the centrifugal ice adhesion test were modelled by the finite elements method. As shown in Fig. 3, the model reproduces the test geometry and dimensions as shown in Fig. 2. Both the ice and the substrate were assumed as linear elastic materials; plasticization of ordinary substrates during the test is indeed not expected. Among the various simulation runs performed in this research, the case for steel and aluminum substrates are presented in this contribution. Additional models were run by assuming the existence of a thin coating layer (modelled as a 200 µm-thick shell) in order to reproduce the actual test conditions as summarized in Table 3. Material properties are summarized in Table 2. The models were meshed using reduced-integration, bilinear, 8-node hexahedral elements and were run using Simulia-Abaqus 6.12-3 and later versions.

Table 2: Material properties for finite element simulations.

Properties	Al	Steel	Coating	Ice [17]
E [GPa]	70	210	0.225	9.332
ν	0.34	0.30	0.40	0.325
ρ [kg/m^3]	2700	7890	4700	919

C. *Other research methods*

Contact angle (CA) measurements were done by using distilled water and KSV CAM200 equipment. A droplet volume of 10 µl was used for static contact angles of superhydrophobic surfaces whereas a volume of 5 µl was used for other surfaces. At least five droplets were used for determining the static contact angle. For dynamic contact angle measurement, the droplets were filled up to 30 µl in 30 s and unfilled at the same rate. The dynamic angles were analyzed once a second. One droplet was used for each sample determining the dynamic contact angles resulting in three parallel measurements for each type of specimen.

Surface properties (surface profile, Ra, Sa values) were analyzed by Alicona Infinite Focus G5 optical profilometer with the 20x objective magnification, resulting in a measurement field size of 0.81 mm x 0.81 mm on the xy-plane. Vertical resolution achieved with this magnification is 50 nm. Ra- and Sa-values were measured from areas as large as possible.

D. *Tested materials*

Several materials and surfaces were selected for the testing. Three hydrophobic and two superhydrophobic coatings were studied (Table 3). Steel was used as a substrate material. Aluminium bulk material was chosen as reference material. It is typical material used in atmospheric conditions and also mainly studied in icing testing by other researchers. PTFE (as a form of tape, making it possible to use a fresh surface for each test) was selected as other reference due to its good non-sticking behaviour.

Table 3: Deposited surfaces and reference materials.

Sample	Coating/surface
H1	PTFE-based hydrophobic coating, Alu Releco
H2	FEP-based hydrophobic coating, Alu Releco
H3	PTFE-based hydrophobic coating, CeraFlon, Alu Releco
SH1	F-containing superhydrophobic hybrid coating, Millidyne
SH2	Superhydrophobic coating, Ultra-Ever Dry®
Al	Reference: Polished aluminum bulk surface
PTFE	Reference: Teflon tape, smooth surface

II. Results and Discussion

Icing behavior of selected coatings and surfaces was studied. Ice adhesion was evaluated and different types of ice were formed. Ice adhesion was compared to the wettability and surface roughness of the surfaces in order to find correlations between icing properties and surface properties.

A. *Icing behavior and ice formation*

Ice was formed in the temperature of -10 ºC. Different ice types were produced by changing icing conditions. Figure 4 presents rime, normal and glaze ice. Soft rime is named as rime ice, glaze ice with no other features than transparency is named as normal ice and glaze ice with distinctive features such as icicles and runback ice is named as a glaze ice.

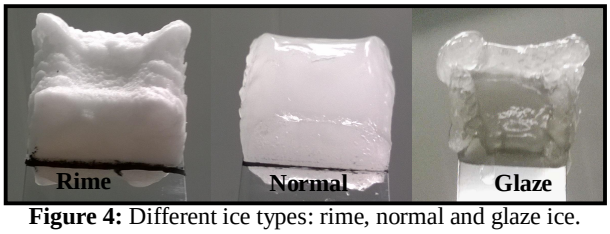

Figure 4: Different ice types: rime, normal and glaze ice.

The different ice types have some characteristic properties, and the types are classified based on their density. According to the standard "ISO-12494", density of soft rime ice varies between 300-600 kg/m^3, hard rime 600-900 kg/m^3 and glaze ice around 900 kg/m^3 [18]. The appearance of soft rime is white, irregularly shaped ice, which has grown against the wind direction. Glaze ice is transparent evenly shaped ice that has runback ice and icicles. The normal ice does not have icicles or runback ice and it is translucent unlike transparent glaze ice.

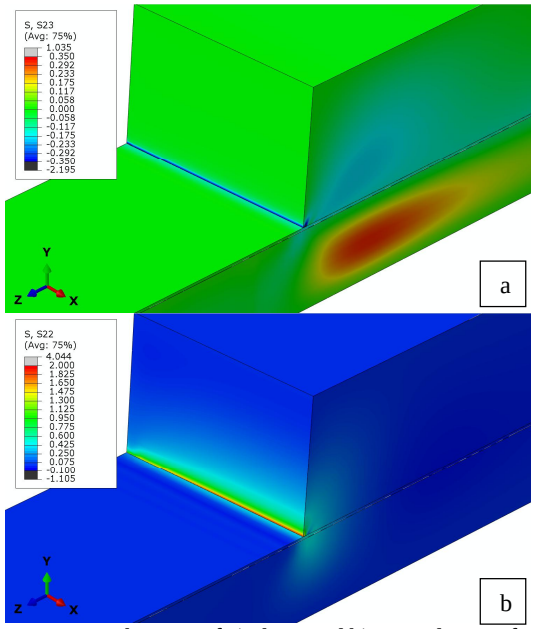

Figure 5: Distributions of a) shear and b) normal stress for an ice block on coated Al substrate.

Finite element simulations confirm that the test method generates maxima of both in-plane shear stress (τ_{23}, Fig. 5a) and out-of-plane normal stress (σ_{22}, Fig. 5b) at the ice-plate interface, regardless of the plate material and of the presence of a thin coating shell. Adhesive failure will therefore occur along such interface, thus minimizing the risks of cohesive failure events, which would act as confounding factors on the test results. It is anyway important to account for the fact that stress maxima along the ice block edge are much larger than they

would be predicted by simple application of the beam theory. This means the detachment of the ice block occurs at larger stress values than those predicted by the analytical equation (2). The actual magnitude of such stresses is a function of the mechanical properties of the involved materials, as these will affect the overall deformation under the action of the centrifugal force. For instance, an elastically compliant substrate (e.g. Al) allows larger elastic bending of the beam under the action of the centrifugal force (Fig. 6a) than a stiffer one (e.g. steel, Fig. 6b) does. The average interface shear stress value at rupture computed according to equation (2) can therefore be assumed as a comparative value, but care should be taken in using this value for quantitative design purposes. Most importantly, the centrifugal ice adhesion test must be run using identical plate material for all samples to be compared, to avoid additional confounding effects on the measured ice adhesion values.

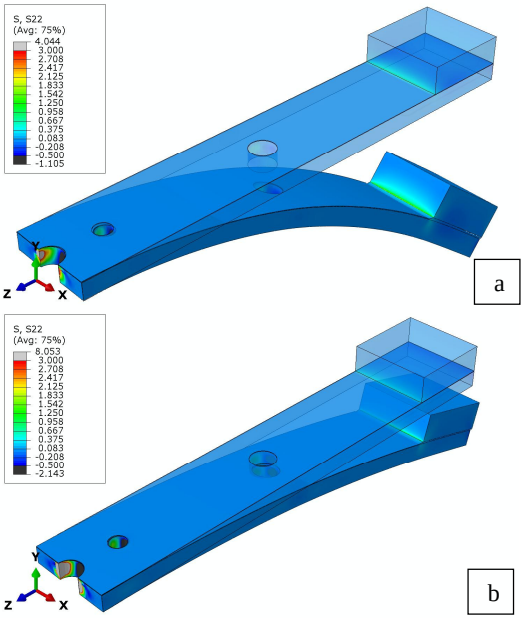

Figure 6: Plots of σ_{22} on original and deformed configuration in the case of a) Al and b) steel substrates. Deformation is enhanced x200 times in both cases.

B. Surface properties

The surface is said to be hydrophobic if the contact angle (CA) is greater than 90º and hydrophilic if the CA is less than 90º. The maximum CA is 180º and minimum 0º. Surfaces with CAs close to these extremes are called either superhydrophobic (>150º) or superhydrophilic (<5º) [19]. The mobility of the droplet may be described by dynamic contact angle parameters: 1) advancing CA is the CA observed at the front end of a moving droplet, 2) receding CA is the CA at the rear end of a droplet and 3) CA hysteresis is the remainder between advancing and receding CAs. A surface with advancing and receding CAs close together has a low CA hysteresis and the droplet easily slides or rolls on the surface.

Table 4 summarizes the static and dynamic CA values. Superhydrophobic SH1 and SH2 coatings had the highest CA values and the lowest hysteresis, which indicates the high mobility of the water droplet. The PTFE reference sample also has relatively low hysteresis although it behaves hydrophobically. Hydrophobic coatings H1 and H2 have similar water droplet behavior whereas H3 has higher CA and also higher hysteresis. H1, H2 and H3 are all fluorine containing polymers, which have been considered to provide low surface energy values. Various fluorine containing coatings have been studied e.g., in [20-22].

Table 4: Contact angle values (CA_Stat: static, CA_Adv: advancing, CA_Rec: receding and Hysteresis) of surfaces.

Ice adhesion increases ↓	Sample	CA_Stat (°)	CA_Adv (°)	CA_Rec (°)	Hysteresis (°)
	PTFE	100	108	92	16
	SH2	165	166	164	2
	SH1	159	165	155	10
	H2	114	123	98	25
	H1	113	116	91	25
	H3	139	148	104	44
	Al	66	80	20	60
Superhydrophobic		Hydrophobic		Hydrophilic	

In addition to the wettability, surface roughness was evaluated. Table 5 presents roughness values Ra (2D values) and Sa (3D values) for the studied samples. Hydrophobic coatings (H1, H2, H3) have different the roughness values. Furthermore, the superhydrophobic coating SH1 has higher roughness compared with the SH2 coating. The surface roughness (Sa) of very smooth Al and PTFE was not measured.

Table 5: Surface roughness values Ra and Sa for the samples measured by using optical profilometer.

Sample	Ra (µm)	Sa (µm)
H1	1.08	3.01
H2	0.61	0.85
H3	9.45	14.28
SH1	2.89	6.84
SH2	0.34	0.7
PTFE	0.14	N/A
Al	0.17	N/A

Figures 7 and 8 present the 3D-surface profiles. In Fig. 7, the surface profiles of the hydrophobic samples, H1, H2 and H3, are presented from the smoothest to coarser surface. The H2 coating has relatively smooth surface containing only fine asperities. The H1 coating has larger variation in the shape of asperities and its surface is consisting of small cavities, which are surrounded by elevated areas creating golf ball-like surface structure. The H3 coating, in turn, has a large variety of different shapes of asperities and its surface is relatively coarse.

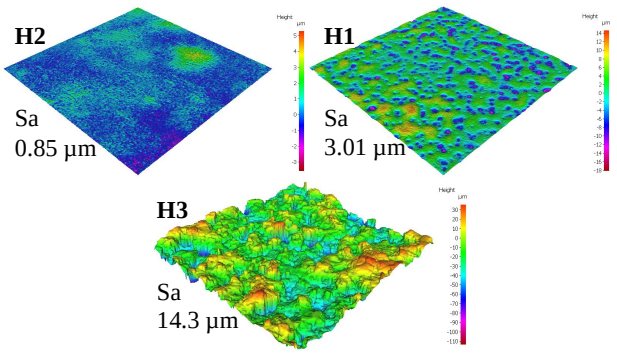

Figure 7: Surface profiles of hydrophobic coatings (H2, H1 and H3).

The 3D-surface profiles of superhydrophobic surfaces are presented in Fig. 8. The surface topographies of these surfaces differ rather significantly from each other. The SH2 coating has relatively smooth surface with only a few higher asperities whereas the topography of the SH1 coating is much coarser, and its surface consists of deep valleys surrounded by either flat or elevated areas. Furthermore, the coarseness of SH1 might have influence on the CA hysteresis of the sample because the water droplet might impinge on the valleys of the surface,

which decreases its mobility (the CA hysteresis of SH1 and SH2 are 10° and 2°, respectively).

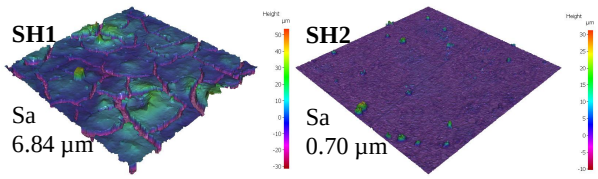

Figure 8: Surface profiles of superhydrophobic coatings (SH1 and SH2).

C. Ice adhesion

Ice adhesion was measured as an average of five measurements. The ice adhesion values with standard deviations are presented in Figure 9. Normal ice was used in this test, which results in the experimental conditions matching closely with the modelled geometry and material properties (Figs. 3,5,6). The uncoated Al plate has the highest ice adhesion whereas PTFE has the lowest. Ice adhesion of superhydrophobic coatings (SH1 and SH2) is close to that of PTFE, indicating good icephobic behavior of superhydrophobic coatings. Icing behavior of hydrophobic coatings H1 and H2 is similar whereas H3 has much higher ice adhesion value.

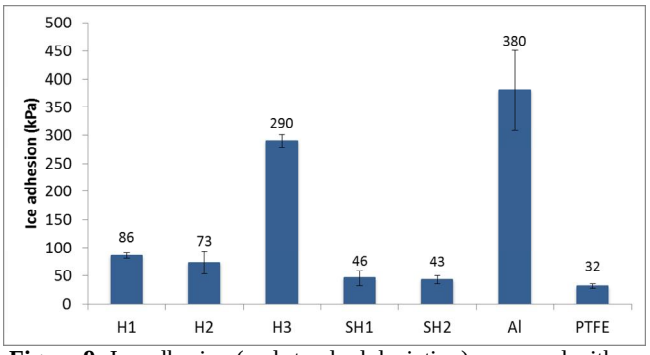

Figure 9: Ice adhesion (and standard deviation) measured with centrifugal ice adhesion test of surfaces.

Relationships between ice adhesion and other surface properties (static CA, hysteresis and surface roughness Ra) are shown in Figure 10. As Fig. 10a indicates, there is no clear relationship between ice adhesion and contact angle (CA). Both superhydrophobic and hydrophobic surfaces can have low ice adhesion values, indicating good icephobicity. Hysteresis vs. ice adhesion, in turn, has clearer connection. This was also noticed in other studies [21, 23]. Surfaces with low hysteresis have lower ice adhesion values (Fig. 10b).

Surface roughness and ice adhesion are also connected. Lower surface roughness usually leads to lower ice adhesion. However, in this study, the surface of the smooth Al plate has low roughness but high ice adhesion, which is due to the material properties. Smooth surface alone does not guarantee low ice adhesion, because other factors such as wettability and surface energy also have impact on adhesion [20,24,25]. PTFE and other fluorine containing polymers are known as low surface energy materials. On the other hand, aluminum has significantly higher surface energy value, which causes high difference in ice adhesion values. [22]

Hydrophobic H1 and H2 coatings showed roughly two times higher ice adhesion values compared to superhydrophobic SH1 and SH2 coatings. Wetting behavior of the droplets has been typically described by Cassie, Wenzel or mixed Cassie-Wenzel states. These tell how the droplets will settle on the surface. In Wenzel state, the liquid will penetrate into the surface roughness whereas in Cassie state, the air will entrapped in the roughness of the surface. The mixed Wenzel-Cassie state is the combination of these two states. [26,27] SH1 and SH2 surfaces are in the Cassie wetting mode due to their high CA and low CA hysteresis. In the Cassie wetting state, the droplets are placed on atop of surface roughness peaks which decrease the ice-solid contact area. The wetting mode of hydrophobic H1 and H2 coatings is, in turn, the mixed Wenzel-Cassie. In this mixed Wenzel-Cassie mode, the droplets can penetrate deeper into cavities of the surfaces creating larger ice-solid contact area. It has been discussed that the larger ice-solid contact area inflicts higher ice adhesion strengths. [19,28,29].

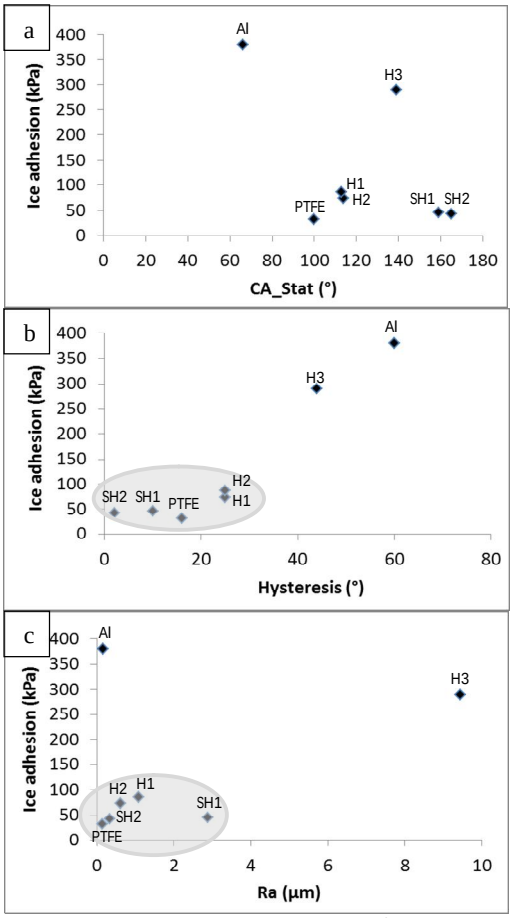

Figure 10: Ice adhesion (IA) versus surface properties: a) IA vs. static contact angle (CA_Stat), b) IA vs. Hysteresis and c) IA vs. surface roughness (Ra).

In literature, one major research approach has been the study of superhydrophobic coatings for the prevention of icing or the minimization of ice adhesion on the surfaces, e.g., in [24,30]. However, opposite opinions have been presented for the speculations of the effectiveness of superhydrophobicity in ice prevention [31,32]. In this study, superhydrophobic coatings showed good icephobic behaviour comparable with PTFE material. However, hydrophobic coatings with low roughness had also relatively good icing behaviour with relatively low ice adhesion values. The surface roughness is a complex phenomenon and suitable texture is dependent on the icing mechanism. Similar to the observations in this study, usually a decrease in roughness reportedly leads to a decrease in ice adhesion [25,33,34].

III. Conclusions

Icing wind tunnel and centrifugal ice adhesion measuring equipment were designed and constructed at TUT. One benefit

of this equipment is that icing conditions can be varied. In addition, different types of ice (rime and glaze ice) can be formed.

In this study, fluoropolymeric coatings taken as examples of hydrophobic and superhydrophobic behavior showed reasonable or low ice adhesion values. These results showed no clear connection between static contact angle and ice adhesion, whereas hysteresis and surface roughness have clearer connection to the ice adhesion. Surfaces with low hysteresis had low ice adhesion. In addition, low surface roughness (except for the smooth Al plate) enables to get lower ice adhesion and thus, better icephobic behavior.

The next research step is to study the effect of different icing conditions and the ice type on the icing properties of the selected surfaces. In the future, the research will be focused on the improvement of wear properties of icephobic coatings.

ACKNOWLEDGMENT

The author would like to thank the staff of the Department of Materials Science, Tampere University of Technology (Tampere, Finland) for helping with a construction of the icing test facilities. This research was done partly in the frame of Hydrobond project (EU, FP7, NMP3-SL-20012-3100531).

REFERENCES

[1] Windpower Engineering and Development, website: http://www.windpowerengineering.com/maintenance/detecting-ice-on-wind-turbine-blades/, cited 6/2015.

[2] P. Guest, Vessel Icing, Mariners Weather Log, 49(3), 2005, 1 p.

[3] L. Cao, A.K. Jones, V.K. Sikka, J. Wu, D. Gao, Anti-Icing Superhydrophobic Coatings, Langmuir, 25(21), 2009, p. 12444–12448.

[4] C.C. Ryerson, Assessment of Superstructure Ice Protection as Applied to Offshore Oil Operations Safety, ERDC/CRREL TR-09-4, 2009, p. 344

[5] P. Kim, T.-S. Wong, J. Alvarenga, M.J. Kreder, W.E. Adorno-Martinez, J. Aizenberg, Liquid-Infused Nanostructured Surfaces with Extreme Anti-Ice and Anti-Frost Performance, ACS Nano, 6(8), 2012, p. 6569–6577.

[6] J. Lv, Y. Song, L. Jiang, J. Wang, Bio-Inspired Strategies for Anti-Icing, ACS Nano, 2014, p. 18.

[7] S. Jung, M. Dorrestijn, D. Raps, A. Das, C.M. Megaridis, D. Poulikakos, Are Superhydrophobic Surfaces Best for Icephobicity?, Langmuir, 27, 2011, p. 3059–3066.

[8] C.C. Ryerson, Ice protection of offshore platforms, Cold Regions Science and Technology, 65, 2011, p. 97–110.

[9] V. Hejazi, K. Sobolev, M. Nosonovsky, From superhydrophobicity to icephobicity: forces and interaction analysis, Scientific Reports, 3(2194), 2013, 6 p.

[10] M.C. Homola, P.J. Nicklasson, P.A. Sundsbø, Ice sensors for wind turbines, Cold Regions Science and Technology, 46, 2006, p. 125–131.

[11] B. Tammelin, K. Säntti, Icing in Europe, BOREAS IV, 1998, p. 125-132.

[12] A.G. Kraj, E.L. Bibeau, Phases of icing on wind turbine blades characterized by ice accumulation, Renewable Energy, 35, 2010, p. 966–972.

[13] C. Peng, S. Xing, Z. Yuan, J. Xiao, C. Wang, J. Zeng, Preparation and anti-icing of supehydrophobic PVDF coating on a wind turbine blade, Applied Surface Science, 259, 2012, p. 764–768.

[14] P. Tourkine, M. Le Merrer, D. Quere, Delayed Freezing on Water Repellent Materials, Langmuir, 25(13), 2009, p. 7214–7216.

[15] F. Arianpour, M. Farzaneh, S.A. Kulinich, Hydrophobic and ice-retarding properties of doped silicone rubber coatings, Applied Surface Science, 265, 2013, p. 546– 552.

[16] C. Laforte, A. Beisswenger, Icephobic Material Centrifuge Adhesion Test, International Workshop on Atmospheric Icing of Structures (IWAIS) XI, Montreal, June 2005, 4 p.

[17] P.H. Gammon, H. Kiefte, J.M. Clouter, W.W. Denner, Elastic Constants of Artificial and Natural Ice Samples by Brillouin Spectroscopy, Journal of Glaciology, 29(103), 1983, p. 433-460.

[18] ISO-12494 standard, Atmospheric icing of structures, The Internatiol Standardization Organization, 2001, p. 56.

[19] X. Zhou, X. Guo, W. Ding, Y. Chen, Superhydrophobic or superhydrophilic surfaces regulated by micro-nano structured ZnO powders, Applied Surface Science, 255, 2008, p. 3371–3374.

[20] S. Farhadi, M. Farzaneh, S. Simard, On Stability and Ice-Releasing Performance of Nanostructured Fluoro-Alkylsilane-Based Superhydrophobic Al alloy2024 Surfaces, International Journal of Theoretical and Applied Nanotechnology, 1(1), 2012, p. 38-44.

[21] S. Kulinich, M. Farzaneh, How wetting hysteresis influences ice adhesion strength on superhydrophobic surfaces, Langmuir , The ACS Journal of Surfaces and Colloids, 25(16), 2009, p. 8854-8856.

[22] S. Yang, Q. Xia, L. Zhu, J. Xue, Q. Wang, Q. Chen, Research on the icephobic properties of fluoropolymer-based materials, Applied Surface Science, 257(11), 2011, p. 4956–4962.

[23] G. Momen, R. Jafari, M. Farzaneh, Ice repellency behaviour of superhydrophobic surfaces: Effects of atmospheric icing conditions and surface roughness, Applied Surface Science, 349, 2015, p. 211–218.

[24] L. Makkonen, Ice Adhesion - Theory, Measurements and Countermeasures, Journal of Adhesion Science Technology, 26, 2012, p. 413–445.

[25] M. Zou, S. Beckford, R. Wei, C. Ellis, G. Hatton, M.A. Miller, Effects of surface roughness and energy on ice adhesion strength, Applied Surface Science, 257, 2011, p. 3786–3792.

[26] R.N. Wenzel, Resistance of solid surfaces to wetting by water, Industrial and Engineering Chemistry, 28, 1936, p. 988-994.

[27] A.B.D. Cassie, S. Baxter, Wettability of porous surfaces, Transactions of the Faraday Society, 40, 1944, p. 546-551.

[28] S. Farhadi, M. Farzaneh, S.A. Kulinich, Anti-icing performance of superhydrophobic surfaces, Applied Surface Science, 257(14), 2011, p. 6264–6269.

[29] G. Fortin, J. Perron, Ice Adhesion Models to Predict Shear Stress at Shedding, Journal of Adhesion Science and Technology, 26(4-5), 2012, p. 523–553.

[30] O. Parent, A. Ilinca, Anti-icing and de-icing techniques for wind turbines: Critical review, Cold Regions Science Technology, 65(1), 2011, p. 88–96.

[31] T. Bharathidasan, S. V. Kumar, M. S. Bobji, R. P. S. Chakradhar, and B. J. Basu, Effect of wettability and surface roughness on ice-adhesion strength of hydrophilic, hydrophobic and superhydrophobic surfaces, Applied Surface Science, 314, 2014, p. 241–250.

[32] S. Kulinich, S. Farhadi, K. Nose, X. W. Du, Superhydrophobic surfaces: are they really ice-repellent?, Langmuir, 27(1), 2011, p. 25-29.

[33] M. F. Hassan, H. P. Lee, S. P. Lim. The variation of ice adhesion strength with substrate surface roughness, Measurement Science and Technology, 21, 2010, 9 p.

[34] M. Susoff, K. Siegmann, C. Pfaffenroth, M. Hirayama, Evaluation of icephobic coatings - Screening of different coatings and influence of roughness, Applied Surface Science, 282, 2013, p. 870–879.